AIAA JOURNAL
Vol. 39, No. 1, January 2001

Mixture Fraction Field in a Turbulent Nonreacting Propane Jet

R. W. Schefer*
Sandia National Laboratories, Livermore, California 94551
and
R. W. Dibble†
University of California, Berkeley, Berkeley, California 94720

Time- and space-resolved mixture fraction measurements have been made throughout a turbulent nonreacting propane jet issuing into coflowing air using laser Rayleigh scattering. The objective of the measurements has been to obtain a better understanding of the flow structure and mixing process in turbulent variable-density jets where turbulent mixing has been decoupled from the effects of chemical heat release found in highly exothermic reacting jets. The measurements yield probability density distributions of the mixture fraction, from which the means, higher moments, and intermittency are calculated. Time histories of the Rayleigh signal are analyzed to obtain the power spectra and autocorrelations. Comparisons are made with results for other constant- and variable-density turbulent jets, and the observed differences are discussed.

I. Introduction

THE development of numerical models for turbulent reacting flows is based largely on submodels developed for nonreacting, constant-density flows. Verification of these submodels is often difficult due to the complex interaction between turbulent mixing and combustion heat release. Previous evidence indicates that the use of submodels based on isothermal or nonreacting turbulent flows may not be valid in reacting flows.[1–3] The turbulent, variable-density, nonreacting jet provides a simplified flow situation in which the complexity of variable density remains without the complex coupling between turbulent mixing and chemical heat release. Thus the effects of variable density on turbulence can be isolated from combustion chemistry. Nonreacting, variable-density flows form a logical bridge between nonreacting constant-density and reacting turbulent flows in which the development of a database is necessary to the development of numerical models for turbulent reacting flows.

Constant-density turbulent jets have been studied extensively,[4–9] and the development of laser diagnostics has led to an increased amount of data in reacting turbulent jets.[10–12] Previous studies on nonreacting constant- and variable-density turbulent flows relevant to the present investigation are summarized in Table 1. Included in Table 1 are studies of air jets into surrounding air where the jet is seeded with smoke particles to provide a tracer for the concentration of fluid originating from the jet,[6,7] heated air jets where temperature is the measured scalar,[13–15] and constant- and variable-density jets where the jet-fluid concentration has been measured using Rayleigh[8,16,17] and Raman scattering.[18] Previous results for a C_3H_8 jet with a low-velocity coflowing airstream were reported by Dyer.[19]

In the present investigation laser Rayleigh scattering is used to obtain time- and space-resolved measurements of mixture fraction in a turbulent nonreacting C_3H_8 jet. Velocity measurements were obtained previously in this flow and are reported elsewhere.[20–22] In Ref. 21 a two-color laser Doppler velocimetry (LDV) system was used to measure the axial and radial components of velocity simultaneously. Velocity measurements conditional on the jet stream and on the coflowing airstream were obtained by seeding each stream independently. It was found that the conditionally averaged statistics can differ significantly in regions where incomplete mixing has occurred between the jet stream and airstream. In Ref. 22 the two-color LDV system was combined with a laser Raman scattering system to obtain simultaneous measurements of velocity and mixture fraction in both the nonreacting C_3H_8 jet and in a reacting jet mixture of hydrogen and argon with coflowing air.

A major objective of this work is the development of a comprehensive database for variable-density turbulent jets through the systematic study of a well-defined flow. Tabulated mixture fraction and velocity data obtained in the present flow can be found on the web as part of the experimental data archives of the International Workshop on Measurements and Computation of Turbulent Nonpremixed Flames.[23]

In the remainder of this paper the experimental system and data reduction techniques are described. Experimentally measured axial and radial profiles of the mean mixture fraction and the higher moments are then presented. Next the probability density distributions of C_3H_8 mixture fraction at various locations in the flowfield are shown. Finally the power spectral density and autocorrelation results are presented.

II. Experimental

A. Test Facility and Experimental Conditions

The measurements were performed in the Sandia Turbulent Diffusion Flame Facility.[22] The facility is a forced-draft vertical wind tunnel with an axisymmetric fuel jet located at the upstream end of the test section and aligned with the test section centerline. The high-velocity central jet of fuel is surrounded by a coflowing airstream. Airflow rates up to 40 m/s (131 ft/s) are provided by a variable-speed centrifugal fan. Flow rates are determined from the measured pressure drop across a calibrated venturi meter located upstream of the test section. A honeycomb section before the contraction cone and a 9:1 area ratio across the contraction cone provide a uniform velocity across the test section entrance with a measured inlet turbulence level of 0.4%. The fuel nozzle has an inside diameter D of 0.526 cm (0.21 in.) and an outer diameter of 0.90 cm (0.35 in.). The jet exit is preceded by a 2-m (6.56-ft) length of straight tubing. Gas flows through the fuel jet are metered by mass flow controllers to an accuracy of 2%.

The test section has a 30-cm (11.8-in.)-square cross section and is 200 cm (75.7 in.) long. Optical access is provided through the removable glass walls of the test section. The test section and contraction cone are mounted on a traversing mechanism driven by stepping motors to provide positioning in three directions. This geometry allows the optical diagnostics to be described to remain fixed and simplifies the alignment procedure.

The C_3H_8 jet bulk velocity u_j in the present investigation was 53 m/s (±0.1 m/s) [174 ft/s (±0.3 ft/s)], giving a Reynolds number based on the jet exit diameter, $Re_j = 6.8 \times 10^4$. Velocity measurements at the test section inlet showed that the maximum velocity at the centerline of the jet exit was 70 m/s (230 ft/s), which is consistent with fully developed, turbulent pipe flow ($u_{j,\max} = 1.28\, u_{j,\text{bulk}}$).

Received 18 February 1999; revision received 31 May 2000; accepted for publication 1 June 2000.

*Senior Member Technical Staff, Combustion Research Facility.
†Professor, Mechanical Engineering Department.

Table 1 Experimental conditions for nonreacting jet data

Flow	ρ_{jet}/ρ_{air}	u_{air}/u_{jet}	$Re \times 10^3$	Reference
C_3H_8–air	1.52	0.174	68	Present data
CH_4–air	0.55	0.08	40	Pitts and Kashiwagi[16]
CH_4–air	0.55	0	16	Birch et al.[18]
C_3H_8–air	1.52	0.033	9.79	Dyer[19]
Air–air	1.0	0	54	Becker et al.[6]
Air–air	1.0	0.024	56.1	Shaughnessy and Morton[7]
		0.042	31.6	
Heated air–air	0.95	0.15	38	Antonia et al.[13]
		0.34	38	
		0.53	38	
Heated air–air	0.94	0	34.1	Chevray and Tutu[14]
He–air	0.13	0	4	Richards and Pitts[17]
CH_4–air	0.55	0	25	
C_3H_8–air	1.52	0	25	
C_2H_2–N_2	1.0015	0	5	Dowling and Dimotakis[8]
C_3H_6–Ar	1.053	0	16	
C_3H_6–Ar	1.053	0	40	
Heated air–air	0.54	0	50	Lockwood and Moneib[15]

The coflowing air velocity u_{air} was 9.2 m/s (±0.1 m/s) [30.2 ft/s (±0.3 ft/s)], which gives a ratio of coflow air to jet velocity of 0.174. Bulk velocity of the fuel jet was determined from the measured volumetric flow rates using a calibrated mass flow controller and the internal area of the jet nozzle. At these flow conditions, the measured value for the axial pressure gradient in the test section was 6 Pa/m at the flow conditions studied.

B. Optical System

Rayleigh scattering measurements were made using a 6-W continuous wave argon-ion laser operating in the single wavelength mode at $\lambda = 488$ nm. The beam was focused with a 35-cm (13.8-in.)-focal-length lens to a 200-μm (0.008-in.) waist diameter. The Rayleigh scattered light was collected at right angles to the incident beam by a 30-cm (11.8-in.)-focal-length $f/2$ collection lens and was relayed to a cooled photomultiplier tube. The measurement volume, defined by the entrance slit to the photomultiplier tube and the laser beam diameter, was 1 mm (0.04 in.) in length by 0.2 mm (0.008 in.) in diameter. The electrical output of the phototube was digitized using an analog-to-digital converter, read, and stored on computer disk. Laser power and the background signal level were recorded at each measurement location, and corrections for any variations in these were applied during the data-reduction procedure.

At each spatial location, 64,000 measurements were taken. The data rate, limited by the transfer rate to the computer, was 16 kHz, so that at each location 4 s of data acquisition were required. This sample rate resulted in frequency components up to 8 kHz contributing to the mean and fluctuating Rayleigh signal.

C. Data Reduction and Error Analysis

Rayleigh scattering has been used to measure concentration, temperature, and density.[24] In a two-component isothermal flow, such as the nonreacting C_3H_8 jet, the Rayleigh signal intensity is directly related to the C_3H_8 mole fraction. The differential cross section σ for Rayleigh scattering by gas molecules is given by

$$\sigma = 2\pi^2(\mu_0 - 1)^2 / n_0\lambda^4 \tag{1}$$

where μ_0 is the index of refraction of the gas at STP, λ is the laser wavelength, n_0 is Loschmidt's number ($2.69 \times 10^{19}/\text{cm}^3$), and a 90-deg scattering angle is assumed. The light intensity I that is scattered by a mixture of gases, with each species having a number density n_i and differential cross section σ_i, is given by

$$I = C_1 \Sigma n_i \sigma_i = C_1 n \Sigma x_i \sigma_i \tag{2}$$

where x_i is the mole fraction of species i and n is the total number density. C_1 is a parameter proportional to the laser intensity, the collection solid angle, and the length of beam imaged on the detector and is determined by calibration. For a binary gas mixture of C_3H_8 and air, Eq. (2) becomes

$$I = C_i n(\sigma_p x_p + \sigma_{air} x_{air}) = C_2[13.5x_p + (1 - x_p)] \tag{3}$$

where x_p and x_{air} are the mole fractions of C_3H_8 and air, respectively, and 13.5 is the ratio of the scattering cross section of C_3H_8 relative to that of air.[19] In the present nonreacting jet, the mixture fraction f is identical to the C_3H_8 mass fraction and is related to x_p by the following equation, which accounts for the molecular weight of air and C_3H_8:

$$f = \frac{x_p mw_p}{x_p(mw_p - mw_{air}) + mw_{air}} \tag{4}$$

The primary sources of error in the Rayleigh scattering measurements were background scattering and shot noise. The major source of background scattering in the present investigation was laser light scattered from the test section windows. Background scattered light was measured at each spatial location by moving the collection optics off the laser beam, thus eliminating the Rayleigh scattered light contribution to the total signal. Using this technique, the background signal was found to be approximately 3% of the Rayleigh signal measured from pure air. At each measurement location, the contribution of background scattering was subtracted from the measured signal. Measurement precision is limited by shot noise in the Rayleigh signal.[16] The estimated standard deviation for single-shot precision of the mixture fraction measurements is 1.5%. The actual uncertainty is effected by potential systematic errors that effect the measurement. The uncertainty of the mixture fraction measurements was estimated from the repeatability of Rayleigh calibration data and from the scatter in measurements for different experimental runs. These uncertainty values are ±2 and ±3% (based on 95% confidence levels) for the mean and fluctuating (rms) mixture fraction, respectively.

III. Results and Discussion

A. Mean and Fluctuating Quantities

The centerline variations in the mean and fluctuating component of the mixture fraction are shown in Fig. 1. Axial distance x is normalized by the jet exit diameter D. The mixture fraction fluctuations $(f'^2)^{1/2}$, hereafter denoted by f', are normalized by the mixture fraction at the centerline f_{cl}. The mean mixture fraction f remains nearly constant over the potential core region, which extends approximately four jet diameters downstream of the jet exit, before decreasing rapidly as coflowing air is entrained by the high-velocity jet and mixes with the C_3H_8. After the initial core region, the fluctuations increase rapidly downstream of the jet exit. In the downstream region, the fluctuations continue to increase but at a slower rate.

The centerline mixture fraction decay for nonreacting jets can be correlated with distance from the virtual origin $x_{0,1}$ (Ref. 16). This correlation can be expressed as

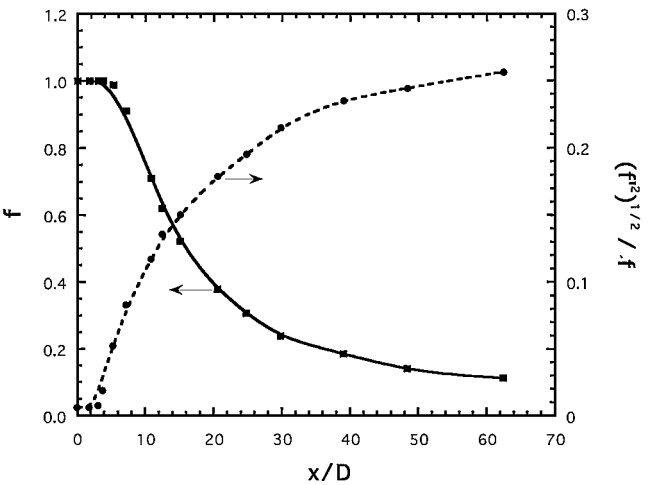

Fig. 1 Mean mixture fraction and mixture fraction fluctuations measured along centerline in turbulent nonreacting C_3H_8 jet.

Table 2 Experimentally determined constants for Eqs. (5) and (6)

Flow	C_1	$x_{0.1}/D$	C_2	$x_{0.2}/D$	Reference
C_3H_8–air	0.185	3.0	0.060	−1.0	Present data
He–air	0.212	3.0	0.113	−0.15	Richards and Pitts[17]
CH_4–air	0.212	3.6	0.115	2.8	
C_3H_8–air					
Pipe	0.208	−2.1	0.108	4.25	
Nozzle	0.210	1.5	0.113	3.6	
C_2H_2–N_2	0.195	−3.7	0.114	——	Dowling and Dimotakis[8]
C_3H_6–Ar	0.211	0.5	0.114	——	
C_3H_6–Ar	0.194	——	0.114	——	
CH_4–air	0.224	−1.0	0.104	0.0	Pitts and Kashiwagi[16]
CH_4–air	0.250	5.8	0.097	0.0	Birch et al.[18]
C_3H_8–air	0.180	0.15	——	——	Dyer[19] (from ref. 16)
Air–air	0.186	2.4	0.106	2.4	Becker et al.[6]

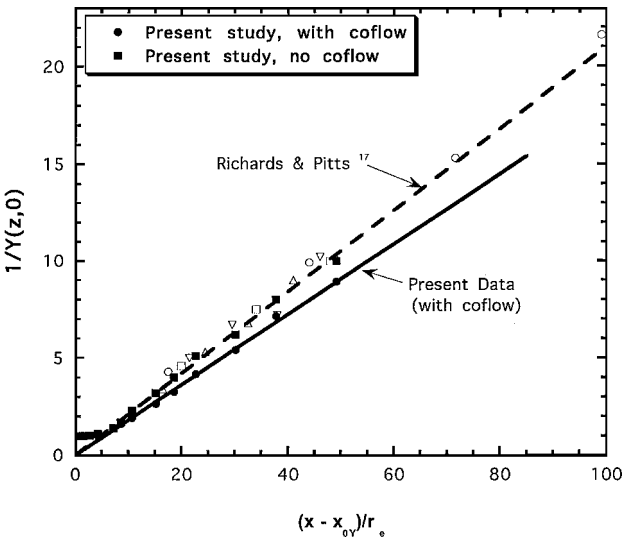

Fig. 2 Reciprocal mean mixture fraction measured along centerline in turbulent nonreacting C_3H_8 jet; present data, C_3H_8 jet with coflow (●) and C_3H_8 jet no coflow (■), and Richards and Pitts,[17] He–air (○), methane–air (□), C_3H_8 pipe (△), and C_3H_8 nozzle (▽).

$$\frac{f_i}{f_{cl}} = \frac{C_1(x - x_{0,1})}{D(\rho_j/\rho_a)^{\frac{1}{2}}} \tag{5}$$

where f_j is the value of the mixture fraction at the jet exit ($f_j = 1$ for pure C_3H_8), ρ_j and ρ_a are the density of the jet and the outer air, and C_1 is a constant. The denominator in Eq. (5) is typically referred to as the effective diameter, $D^* = D(\rho_j/\rho_a)^{1/2}$. Recent experimental results show that C_1 is independent of (ρ_j/ρ_a) (Ref. 17). The centerline variation in the reciprocal mean mixture fraction is replotted in Fig. 2 as a function of normalized distance from the virtual origin $(x - x_{0,1})/D^*$. Also shown for comparison are published experimental results from the variable-density jets of Richards and Pitts,[17] which show a collapse of the data for He–air, CH_4–air, and C_3H_8–air jets onto a single curve when plotted in this form. The present results for C_3H_8 clearly fall below the results of Richards and Pitts,[17] which indicate a slower centerline decay.

Further comparisons of C_1 and $x_{0,1}$ are shown in Table 2. The results of the present investigation give the location of the virtual origin at $x/D = 3.0$ and a value for $C_1 = 0.185 \pm 0.01$. The values of $x_{0,1}$ listed in Table 2 show considerable scatter. Such variations are not unexpected because the location of the virtual origin is sensitive to initial conditions, which are likely to vary between experiments. The values of C_1 also show considerable scatter. This scatter is particularly evident in the results of earlier studies. The more recent studies in Table 2 indicate an average value for C_1 near 0.21 over a wide range of Reynolds number and (ρ_j/ρ_a) (Refs. 8 and 17). The reduced scatter in the more recent studies in likely due to more accurate experimental techniques and to measurements over a larger range of experimental conditions being carried out in single flow configurations, thus eliminating variations in inlet and boundary conditions.

The value for C_1 measured in the present study is about 10% lower than other recent studies show. Given the good collapse of the variable-density jet data of Richards and Pitts[17] and the good agreement in values of C_1 from their results and the constant-density jet data of Dowling and Dimotakis,[8] the inability of Eq. (1) to collapse the present data onto the same curve is likely due to the effects of coflow air. This may account for the good agreement between the value of $C_1 = 0.185$ obtained from the present data and the value of 0.180 obtained by Dyer[19] in a C_3H_8 jet with coflow, although at a lower velocity. From Tables 1 and 2 it can be seen that all literature studies giving consistent values of C_1 had little or no coflow air ($u_{air}/u_{jet} < 0.08$), whereas for the present study $u_{air}/u_{jet} = 0.174$. To verify the effects of coflow air, the measurements were repeated for a C_3H_8 jet at the same jet velocity but without coflow air. The results, shown in Fig. 2, are in good agreement with the literature results for no coflow. Further evidence is provided by velocity measurements in constant-density air jets, which show a decrease in the centerline velocity decay rate as the coflow air velocity is increased.[25,26]

A comparison of the centerline mixture fraction fluctuation intensity, f'/f_{cl}, with results from the literature is shown in Fig. 3. This quantity is often referred to as unmixedness. Data points are included for the CH_4–air jets of Birch et al.[18] and Pitts and Kashiwagi.[16] Values for the asymptotic limit in f'/f_{cl}, attained at downstream locations in the constant-density jets of Dowling and Dimotakis[8] and the variable-density jets of Richards and Pitts,[17] are indicated by horizontal lines. The results from the latter studies show good agreement with the asymptotic value of $f'/f_{cl} = 0.23$ reported for jets with gas density ratios ρ_j/ρ_a varying from 0.14 to 5.11 (Ref. 27). Richards and Pitts[17] further concluded that the asymptotic centerline value for unmixedness is independent of jet density ratio. The initial increase in fluctuation intensity is considerably more rapid for the CH_4–air jets. This observation is consistent with the results showing that flows with higher Reynolds number require longer downstream distances to achieve asymptotic behavior.[28] Note that $Re = 6.8 \times 10^4$ for the present C_3H_8 jet, which is considerably higher than the other studies.

At downstream locations, the present C_3H_8 jet data do not exhibit asymptotic behavior over the range of distances shown and, in fact, continue to increase above the asymptotic values reported in the literature. Again it can be speculated that the higher values of f'/f_{cl} in the present study are due to the presence of coflow. Support for this conclusion can be found in centerline velocity data for constant-density jets, where increasing the ratio of u_{air}/u_{jet} from 0.1 to 0.2 (note that $u_{air}/u_{jet} = 0.174$ for the present jet) increased the asymptotic values for the longitudinal velocity fluctuations from 0.295 to 0.33 (Ref. 25). These values are higher than the value of 0.28 reported for an axisymmetric free jet.[4] Additional evidence is provided

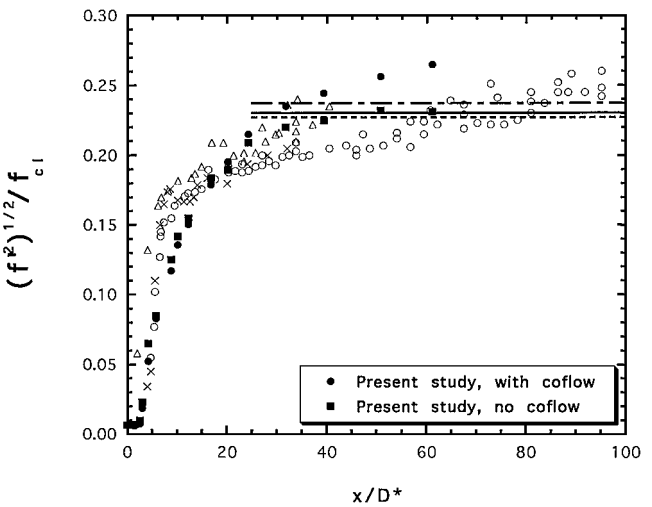

Fig. 3 Mixture fraction fluctuations measured along centerline in turbulent nonreacting propane jet: present data, C_3H_8 jet with coflow (●) and C_3H_8 jet no coflow (■); Dowling and Dimotakis,[8] $Re = 5 \times 10^3$ (——) and $Re = 1.6 \times 10^4$ (- - -); Richards and Pitts,[17] (- - - -); Becker et al.,[6] (×); Pitts and Kashiwagi,[16] (△); and Birch et al.[18] (○).

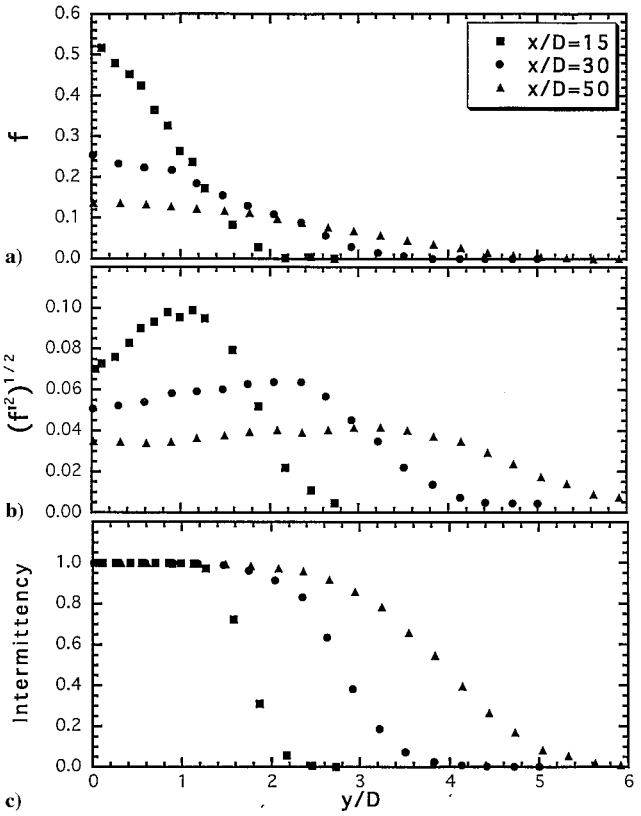

Fig. 4 Radial profiles for a turbulent nonreacting C_3H_8 jet, present data: $x/D = 15$ (■), $x/D = 30$ (●), and $x/D = 50$ (▲): a) mean mixture fraction, b) mixture fraction fluctuations, and c) intermittency.

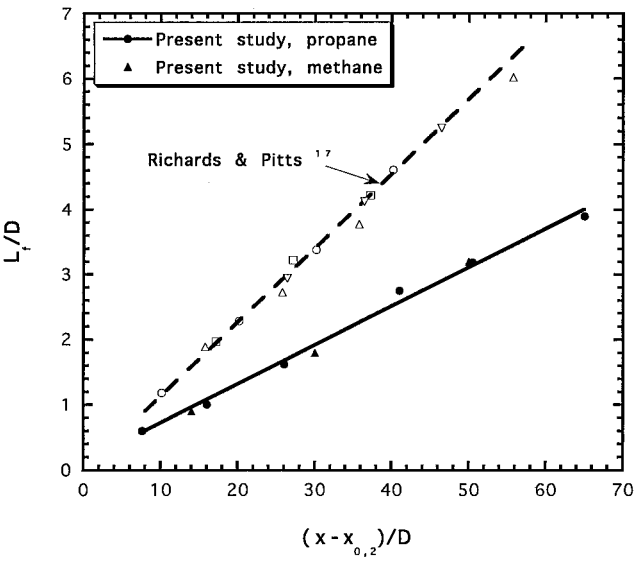

Fig. 5 Variation of mixture fraction half radius with axial distance, present data, C_3H_8 jet with coflow (●) and methane jet with coflow (▲); Richards and Pitts,[17] He–air (○), methane–air (□), propane pipe (△), and propane nozzle (▽).

by measurements in the present C_3H_8 jet without coflow air, which show good agreement with literature results for no coflow. Further studies on the effect of coflow on the asymptotic values for both mixture fraction and velocity fluctuations are clearly needed due to the lack of experimental data.

Radial profiles of f and f' are shown in Figs. 4a and 4b at axial locations of $x/D = 15, 30$, and 50. At each axial location, the maximum mixture fraction occurs at the centerline and decreases outward toward the coflowing air. Consistent with the results in Fig. 1, the centerline value of f decreases in the downstream direction due to mixing with the surrounding air. Maximum fluctuations occur in the mixing region between the jet fluid and the coflowing air where the gradient in f is largest. The fluctuations decrease both near the centerline and farther out toward the airstream. At increasing distance downstream, the maximum fluctuations decrease due to the less intense mixing as the variation in f across the mixing region decreases.

Radial variations in the intermittency γ are shown in Fig. 4c. Here the intermittency is defined as the fraction of time that the mixture fraction is greater than a near-zero threshold (a value of zero corresponding to pure air). Typical probability density distributions (see following section) in the mixing region where $0 < \gamma < 1$ consist of an intermittency spike associated with unmixed air and a broader distribution corresponding to mixed air and C_3H_8. The finite width of the intermittency spike often requires the somewhat arbitrary selection of a threshold value to differentiate between unmixed and mixed fluid. It has been shown that the finite width of the intermittency spike can be closely fitted by a Gaussian, and the area under the resulting curve provides a good estimate of $(1 - \gamma)$ (Ref. 29). The threshold value of mixture fraction determined using this method was $f_{th} = 0.015$. Thus, for $f < 0.015$, the flow is considered as unmixed air, and for $f > 0.015$, the flow is considered as mixed C_3H_8 and air. Calculated values of γ are found to be insensitive to small variations in the threshold level (± 0.005).

At all axial locations, a region exists near the centerline in which γ is unity, which indicates that turbulent mixing is insufficient to transport unmixed air into the central region. Only in a relatively well-defined mixing region for which γ is between 0 and 1 is the presence of any unmixed air observed. Thus, the mixing region can be characterized as consisting of mixed C_3H_8 and air and of unmixed air that is entrained by the high-velocity jet. No unmixed air exists near the centerline at the axial locations shown. All of these observations are consistent with the view that the center of the jet is relatively well mixed, whereas at increasing radii, engulfment of coflowing air and subsequent mixing occurs.

The jet spreading rate can be determined from the mean mixture fraction profiles and is typically characterized by the mixture-fraction half-radius L_f, defined as the radial location at which the mixture fraction is equal to half its centerline value. The variation in L_f (normalized by the jet exit diameter) with axial distance is shown in Fig. 5. For distances sufficiently far downstream, L_f is proportional to the distance from a virtual origin $x_{0,2}$ (Refs. 16 and 17). This dependence can be written as

$$L_f/D = C_2[(x - x_{0,2})/D] \tag{6}$$

A fit of the present data in Fig. 5 (solid line) gives a value of $x_{0,2}/D = -1$ and $C_2 = 0.060 \pm 0.005$. The spreading rate obtained in the present study is considerably less than that measured in variable-density jets with no coflow (dashed line) (Ref. 17). Values of $x_{0,2}$ and C_2 obtained from the literature are also listed in Table 2. The spreading rates for the variable-density jets of Richards and Pitts[17] and the constant-density jets of Dowling and Dimotakis[8] show good agreement, indicating the jet spreading rate is independent of density ratio. The spreading rate of the present C_3H_8 jet is approximately 40% lower. It is again likely that this difference is attributable to the coflow air. Velocity measurements in a constant-density jet with comparable coflow show a similar decrease in the jet-spreading rate with increasing coflow velocity.[25,26]

Variations in f and f' are shown in Figs. 6a and 6b as a function of radial distance normalized by L_f. Note that the use of similarity variables such as L_f is not meant to imply that flow similarity exists in variable-density jets with high coflow air velocities, but rather to emphasize differences with other jet flows in the literature. Shown for comparison as a solid line is a similarity profile based on a best fit to the constant-density jet data of Dowling and Dimotakis.[8] The dashed line in Fig. 6a is a Gaussian-type function of the form

$$f/f_{cl} = \exp\left[-0.693(y/L_f)^2\right] \tag{7}$$

Equation (7) has been shown to provide a good fit to data in CH_4–air jets[16] and shows good agreement with the variable density data of Richards and Pitts[17] (dotted line, Fig. 6). It also provides a good fit to the present data for $y/L_f < 1.25$. At larger values of y/L_f, the

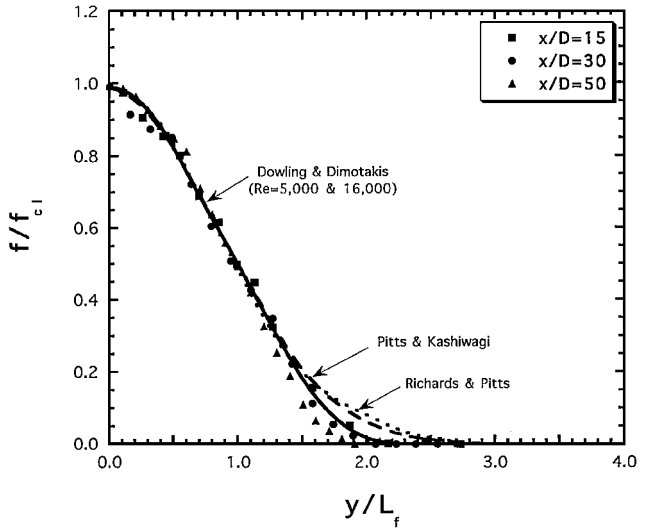

a) Mean mixture fraction

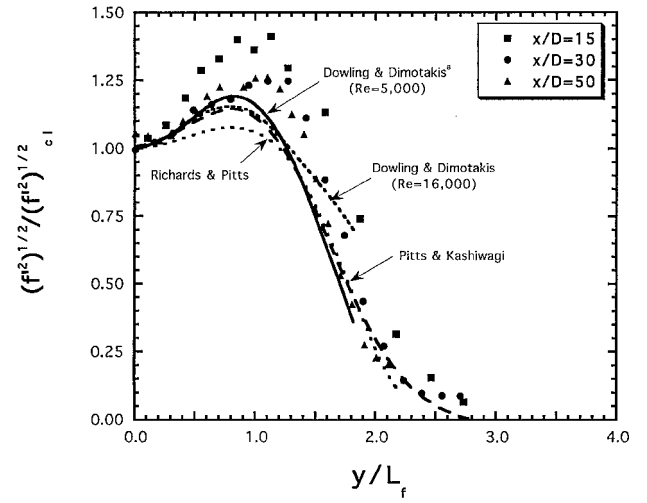

b) Mixture fraction fluctuations

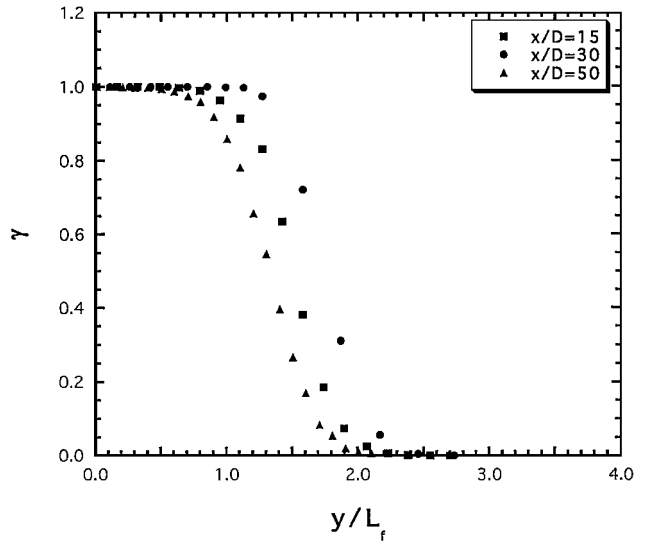

c) Intermittency

Fig. 6 Normalized radial profiles for a turbulent nonreacting C_3H_8 jet, present data: $x/D = 15$ (■), $x/D = 30$ (●), and $x/D = 50$ (▲); Dowling and Dimotakis,[8] $Re = 5 \times 10^3$ (——) and $Re = 1.6 \times 10^4$ (- - - -); Pitts and Kashiwagi,[16] (– – –); and Richards and Pitts[17] (- - - -).

Table 3 Experimentally determined constants for Eqs. (5) and (6)

Flow	f'_{max}/f	y_{max}/L_f	Reference
C_3H_8–air	1.24	0.96	Present data
He–air	1.08	0.81	Richards and Pitts[17]
CH_4–air	1.08	0.81	
C_3H_8–air	1.08	0.81	
Constant density	1.196	0.83	Dowling and Dimotakis[8]
C_3H_8–air	1.29	0.80	Dyer[19] (from ref. 16)
CH_4–air	1.18	0.70	Pitts and Kashiwagi[16]
CH_4–air	1.20	0.70	Birch et al.[18]
Air–air	1.15	0.80	Becker et al.[6]
Air–air	1.14	——	Shaughnessy and Morton[7]
Heated air–air	1.26	0.90	Lockwood and Moneib[15]

decrease in f with radial distance is more rapid than Gaussian and is in better agreement with the Dowling and Dimotakis data.[8]

The mixture-fraction fluctuations normalized by the centerline value f'/f'_{cl} are shown in Fig. 6b. The profile at $x/D = 15$ shows consistently higher fluctuations than at the downstream locations for all radial locations. At $x/D = 30$ and 50 the profiles show good similarity for $y/L_f < 1$, but at larger radial distances the profile at $x/D = 50$ falls slightly inside the results for $x/D = 30$. This result could be due to the effects of the coflowing airstream because radial CH_4 concentration profiles at $x/D = 20$, 30, and 40 in a CH_4–air jet with no coflowing air show good similarity with respect to the normalized radial distance y/L_f (Ref. 18).

Also shown in Fig. 6b are fitted curves based on results from the literature. Dowling and Dimotakis[8] observed a Reynolds number dependence of the concentration fluctuation profiles in constant-density jets in which an increase in the Reynolds number causes a broadening of the profile. The effect was attributed to diffusional smoothing of the concentration field at the edge of the jet. Based on timescale arguments, it was speculated that increasing the Reynolds number decreases the amount of diffusional smoothing and increases the local concentration fluctuations. The good agreement between the high Reynolds number jet of the present study and the lower Reynolds number jets of Refs. 16 and 17 indicate no such dependence.

A comparison of the maximum fluctuations f'_{max} and their radial locations is shown in Table 3. The scatter in the data, even in more recent studies, makes it difficult to reach any conclusions. Previous measurements have shown that the scalar fluctuations are independent of variable density effects.[17] Thus, the scatter between the variable-density and constant-density jets in Table 3 appears to be due to experimental uncertainty. However, the good similarity shown by the profiles at $x/D = 30$ and 50 for the present C_3H_8 jet do seem to indicate higher maximum fluctuations and a shift in the location of this maximum with respect to L_f. Given that the other jets shown in Fig. 6b have either very low or no coflow, this may be attributable to the presence of coflow in the C_3H_8 jet. The higher fluctuations with coflow are consistent with the higher velocity fluctuations measured in the shear layer of constant-density jets with coflow.[25]

Consistent with the normalized mean and fluctuating mixture fraction profiles, the intermittent mixing region (Fig. 6c) shifts toward the centerline with respect to the half-radius L_f. This shift is be expected because the turbulence structure has not yet reached a self-preserving state and the turbulence length scale, as given by the mean position of the mixing region ($\gamma = 0.5$), is changing with respect to the length scale of the mean flow L_f.

B. Higher Moments

Radial variations in the third and fourth moments of the mixture fraction (skewness S and kurtosis K, respectively) are shown in Figs. 7a and 7b. The values of S and K for a Gaussian distribution are 0.0 and 3.0, respectively. At the centerline, the skewness has a slightly negative value at all axial locations. Outward from the centerline, S increases at first slowly, followed by a rapid increase at the outer edge of the mixing layer. The kurtosis initially decreases to a minimum value of 2.8 at a radial location just inside the mixing region before rapidly increasing as the outer airflow is approached.

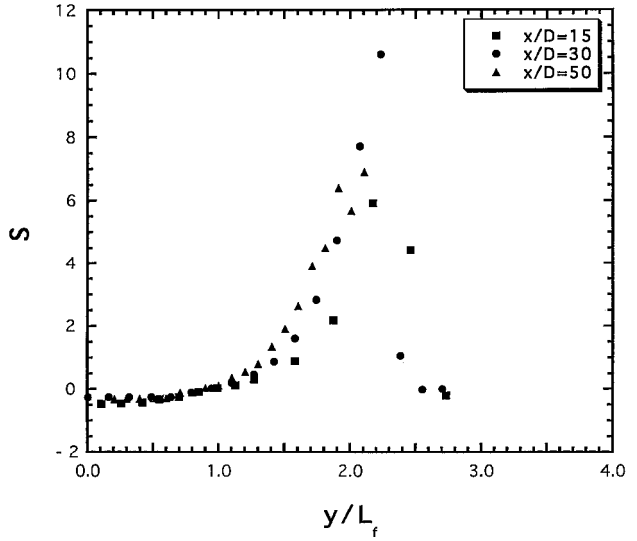

a) Skewness

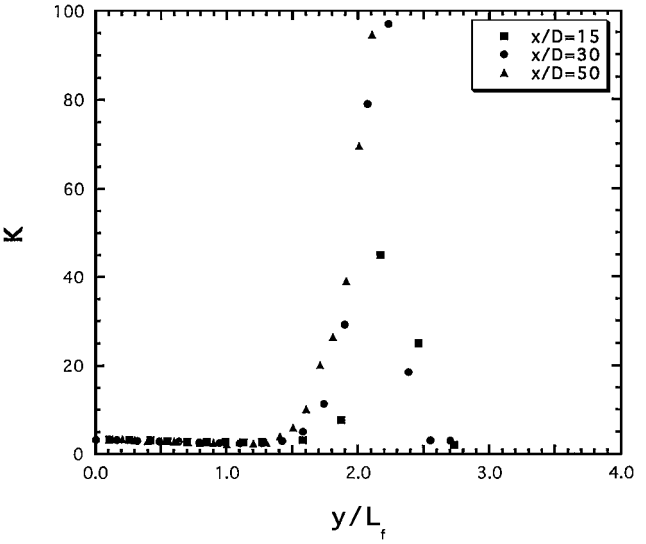

b) Kurtosis

Fig. 7 Normalized radial profiles for a turbulent nonreacting C_3H_8 jet, present data: $x/D = 15$ (■), $x/D = 30$ (●), and $x/D = 50$ (▲).

The rapid increase in S and K in the intermittent mixing region is due to the passage of unmixed air past the measurement volume. This results in periods of time during which the mixture fraction is zero and causes a sharp cutoff in the mixture fraction probability distribution at $f = 0$. Hence, K must increase rapidly as the fraction of time during which pure air is present increases. These results are in good agreement with data in air–air jets,[15] heated jets,[13] and CH_4–air jets.[16,18]

The centerline variation in S and K can also be obtained from Fig. 7. The present results show the skewness increasing from -0.45 at $x/D = 15$ to -0.31 at $x/d = 50$. Pitts and Kashiwagi[16] found a comparable increase in S with axial distance for a CH_4–air jet ($S = -0.6$ at $x/d = 20$ and $S = -0.35$ at $x/D = 60$), whereas Birch et al.[18] measured a relatively constant value of $S = -0.3$ along the centerline. The reason for the difference in centerline behavior between these studies is not clear; however, the measurement of a non-Gaussian negative skewness along the centerline is consistent in both the C_3H_8–air jet and the CH_4–air jets. In the present study, K shows a small decrease with axial distance from 3.4 at $x/D = 15$ to 3.1 at $x/D = 50$. These results are in good agreement with the range of values obtained in CH_4–air jets.[16,18]

C. Probability Density Distributions

Probability density distributions of the mixture fraction $p(f)$ were calculated from 8000 measurements at each spatial location using 50 bins equally spaced over the 3-σ limits of the data. The

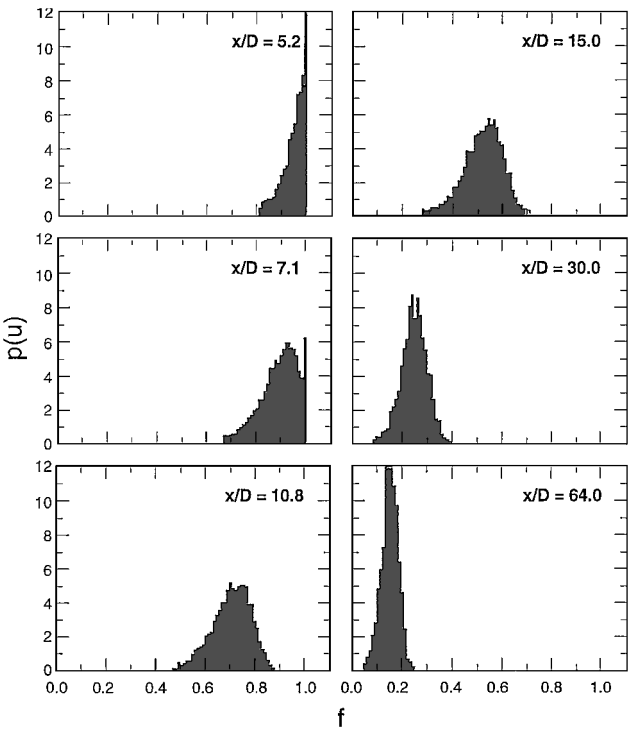

Fig. 8 Probability density distributions of mixture fraction along the centerline of a turbulent nonreacting C_3H_8 jet.

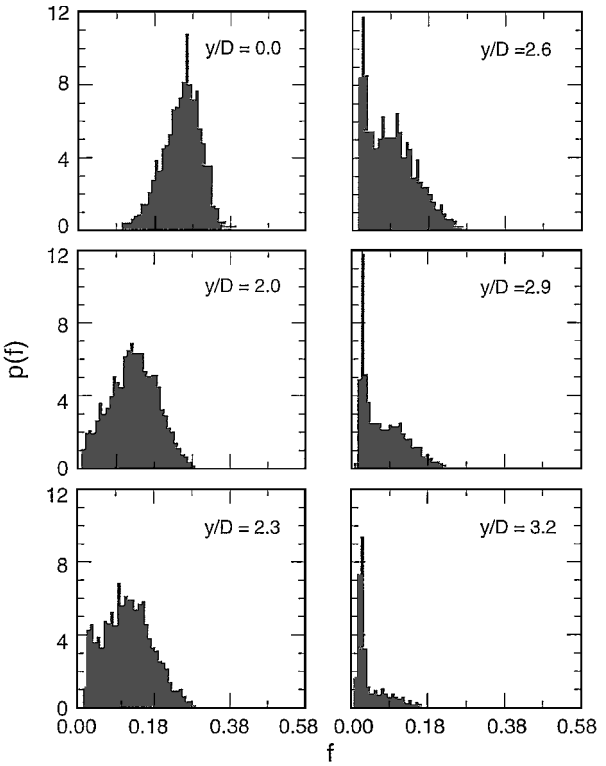

Fig. 9 Probability density distributions of mixture fraction for a turbulent nonreacting C_3H_8 jet at an axial location of $x/D = 30$.

distributions have been normalized so that the following relation is valid:

$$\int_0^1 p(f)\,\mathrm{d}f = 1$$

The evolution of $p(f)$ along the centerline is shown in Fig. 8. Nearest the jet exit ($x/D = 5.2$), the distribution consists of a peak at $f = 1$ corresponding to pure C_3H_8 and a contribution at $f < 1$ corresponding to mixed C_3H_8 and air. Downstream the contribution from pure C_3H_8 decreases as air is entrained by the jet and mixes

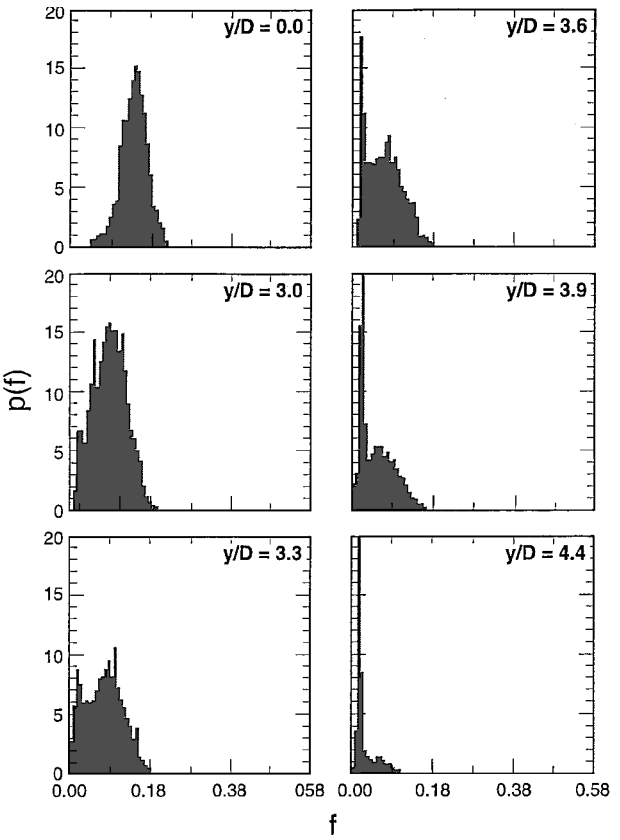

Fig. 10 Probability density distributions of mixture fraction for a turbulent nonreacting C_3H_8 jet at an axial location of $x/D = 50$.

with the jet fluid. At $x/D = 10.8$, the contribution from pure C_3H_8 has disappeared, and the distribution becomes more Gaussian-like, although some skewing toward lower values of f is apparent. Farther downstream, $p(f)$ shifts to lower values of f with increasing axial distance due to continued mixing with coflowing air. The skewness in the distribution persists at downstream locations but appears to be gradually decreasing. Deviations from Gaussian statistics along the centerline have also been observed in CH_4–air jets.[18] No evidence of any pure air can be seen in distributions as far as 64 diameters downstream.

Radial variations in $p(f)$ are shown in Figs. 9 and 10 for $x/D = 30$ and 50, respectively. These distributions are qualitatively similar to conserved scalar distributions observed in constant- and variable-density jets.[8,18] Near the centerline, the distributions are dominated by a broad, Gaussian-like distribution corresponding to a turbulent mixture of C_3H_8 and entrained air, whereas at outer radial locations, a sharp spike corresponding to pure air at $f = 0$ is observed. In the mixing region ($0 < \gamma < 1$) the distribution is bimodal and consists of contributions from both the unmixed air and mixed C_3H_8 and air. At the axial locations shown, no pure propane is indicated ($f = 1$) because sufficient entrainment of coflowing air and mixing has occurred upstream. The smooth transition between the air spike and the broader distribution corresponding to mixed fluid has been attributed to the existence of a viscous superlayer between the unmixed air and the mixed C_3H_8 and air zones and has led to a proposed composite distribution that includes unmixed air, fully mixed C_3H_8 and air, and a contribution from the viscous superlayer.[29]

D. Autocorrelation and Power Spectra

The autocorrelation functions and power spectra were calculated from the time records of the digital data using a Fourier transform. In the present study, the number of samples in each time record (at each spatial location) was 64,000. Digital noise in the power spectra was

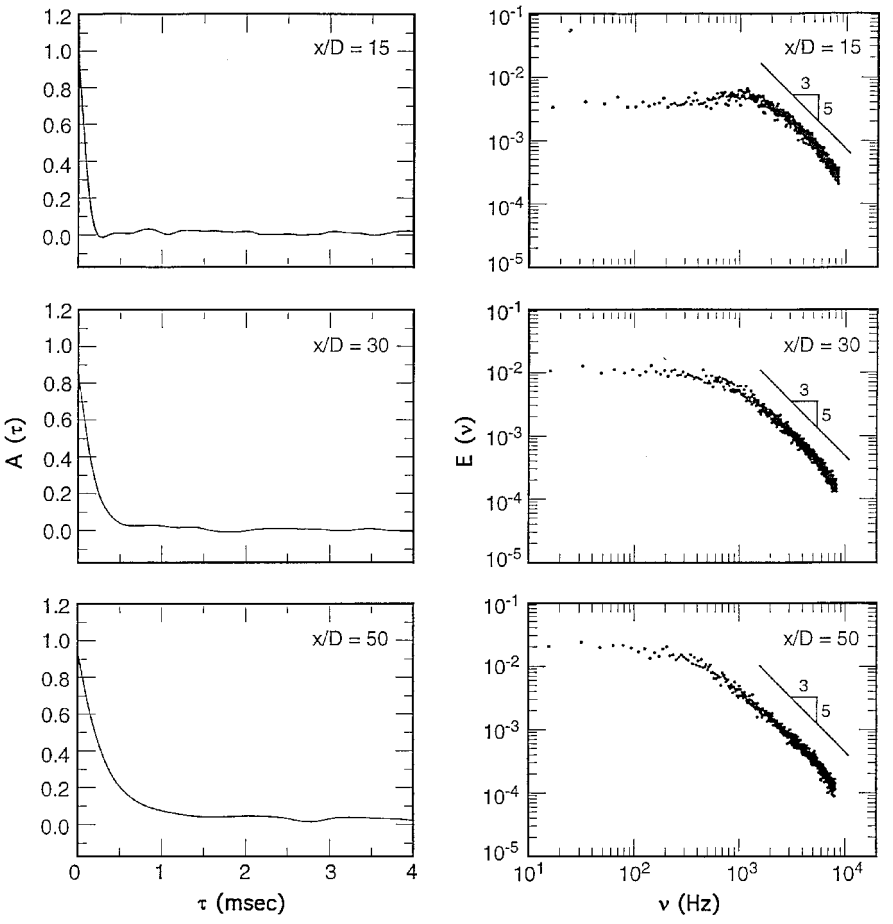

Fig. 11 Autocorrelation function (left column) and power spectra (right column) for a turbulent nonreacting C_3H_8 jet measured along the centerline.

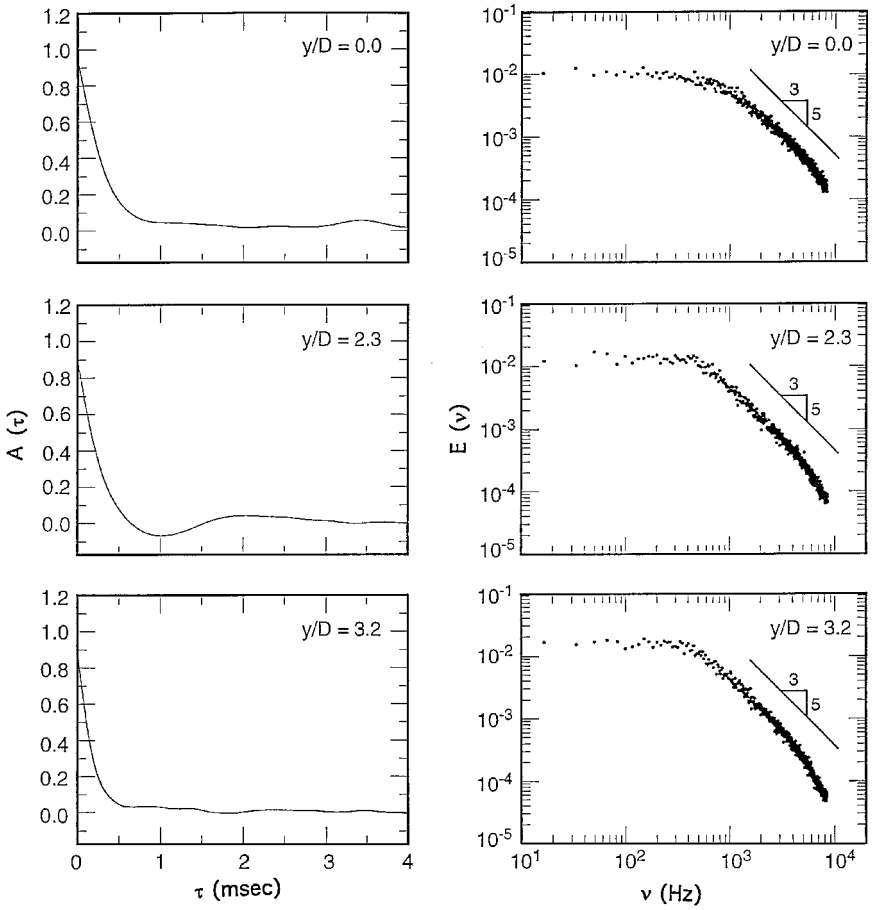

Fig. 12 Autocorrelation function (left column) and power spectra (right column) for a turbulent nonreacting C_3H_8 jet at an axial location of $x/D = 30$.

reduced by grouping the data into records of 4096 data points and averaging the Fourier transforms of these shorter records.[18] Calculated autocorrelation functions and power spectra along the centerline are presented in Fig. 11, which shows the autocorrelation function $A(\tau)$ as a function of delay time τ and the power spectral density $E(\nu)$ as a function of frequency ν. The Nyquist cutoff frequency of 8 kHz corresponds to the maximum data rate of 16 kHz, which was limited by the read and convert time of the analog-to-digital converter. At the upstream location of $x/D = 15$, there is still some spectral energy due to turbulent fluctuations at frequencies above the cutoff frequency. However, further analysis shows that only about 3% of the spectral density occurs above 8 kHz. Both the power spectra and the autocorrelation functions show a shift in the energy distribution to lower frequencies in the downstream direction. The power spectra also display the expected $-\frac{5}{3}$ power law region for the scalar fluctuations observed in constant- and variable-density jets.[8,18] The distributions along the centerline correspond to random turbulent fluctuations with no dominant frequencies.

Typical radial variations are shown in Fig. 12 for $x/D = 30$. The power spectra at outer radial locations show an extended power law region, in agreement with measurements in constant-density jets.[8] Generally, the spectra are nearly flat at the lower frequency end with the possible exception of a mild peak between 500 and 1000 Hz at $y/D = 2.3$. No evidence of any well-defined periodic oscillations exists.

IV. Conclusions

Measurements of the mixture fraction field have been obtained throughout a turbulent, variable-density C_3H_8 jet with coflowing air. From these measurements axial and radial variations in the means and higher moments of the mixture fraction and the probability density distributions have been determined. Power spectra and autocorrelations have been calculated from the time histories of the digitized data and are also presented.

A comparison of the present data with results in the literature for constant- and variable-density jets with little or no coflow reveals significant differences. In particular, both the centerline decay and the jet-spreading rate are higher in the present jet. The scalar fluctuation intensities along the centerline also attain higher values at comparable downstream locations and, over the range of axial distances studied, the fluctuation intensities do not approach an asymptotic limit. These results are attributed to the presence of a coflowing airstream.

Radial variations in the mean mixture fraction and the higher moments do not display similarity when radial location is normalized by the mixture fraction half radius for $x/D < 50$, although an approach to similarity at greater downstream distances is indicated.

Probability density distributions along the centerline indicate that pure C_3H_8 disappears beyond approximately 10 diameters of the jet exit due to mixing with entrained air. Farther downstream, the distributions deviate from Gaussian statistics and are negatively skewed toward lower values of mixture fraction. Probability density distributions measured at different radial locations consist of an unmixed air spike at outer radial locations and a relatively broad Gaussian-like distribution near the centerline where the C_3H_8 and air are well mixed. In the intermittent mixing region, the distributions are bimodal and are well characterized by the sum of an intermittency spike corresponding to unmixed air and a broader distribution corresponding to mixed C_3H_8 and air. The non-Gaussian distribution corresponding to mixed C_3H_8 and air in the intermittent mixing region indicates a contribution from the viscous superlayer located between the unmixed air and mixed C_3H_8 and air zones.

Acknowledgment

This research was supported by the U.S. Department of Energy, Office of Basic Energy Sciences, Division of Chemical Sciences.

References

[1] Yanagi, T., and Mimura, Y., "Velocity–Temperature Correlation in Premixed Flame," *Eighteenth Symposium (International) on Combustion*, Combustion Inst., Pittsburgh, PA, 1980, pp. 1031–1039.

[2]Moss, J. B., "Simultaneous Measurements of Concentration and Velocity in an Open Premixed Turbulent Flame," *Combustion Science and Technology*, Vol. 22, No. 1, 1980, pp. 119–129.

[3]Driscoll, J. F., Schefer, R. W., and Dibble R. W., "Mass Fluxes Measured in a Turbulent Nonpremixed Flame," *Nineteenth Symposium (International) on Combustion*, Combustion Inst., Pittsburgh, PA, 1982, pp. 477–485.

[4]Wygnanski, I., and Fiedler, H., "Some Measurements in the Self-preserving Jet," *Journal of Fluid Mechanics*, Pt. 3, Vol. 38, 1969, pp. 577–612.

[5]Antonia, R. A., and Bilger, R. W., "An Experimental Investigation of an Axisymmetric Jet in a Co-Flowing Air Stream," *Journal of Fluid Mechanics*, Pt. 4, Vol. 61, 1973, pp. 805–822.

[6]Becker, H. A., Hottel, H. C., and Williams, G. C., "The Nozzle-Fluid Concentration of the Round Turbulent Free Jet," *Journal of Fluid Mechanics*, Vol. 30, Dec. 1967, pp. 285–303.

[7]Shaughnessy, E. J., and Morton, J. B., "Laser Light-Scattering Measurements of Particle Concentration in a Turbulent Jet," *Journal of Fluid Mechanics*, Pt. 1, Vol. 80, 1977, pp. 129–148.

[8]Dowling, D. R., and Dimotakis, P. E., "Similarity of the Concentration Field of Gas-Phase Jets," *Journal of Fluid Mechanics*, Vol. 218, 1990, pp. 109–141.

[9]Dowling, D. R., Lang, D. B., and Dimotakis, P. E., "An Improved Laser-Rayleigh Scattering Photodetection System," *Experiments in Fluids*, Vol. 7, No. 7, 1989, pp. 435–440.

[10]Starner, S. H., Bilger, R. W., Dibble, R. W., and Barlow, R. S., "Piloted Diffusion Flames of Diluted Methane Near Extinction: Mean Structure from Raman/Rayleigh Fluorescence Measurements," *Combustion Science and Technology*, Vol. 70, No. 4–6, 1990, pp. 111–133.

[11]Barlow, R. S., Dibble, R. W., Starner, S. H., and Bilger, R. W., "Piloted Diffusion Flames of Nitrogen-Diluted Methane Near Extinction: OH Measurements," *Twenty-Third Symposium (International) on Combustion*, Combustion Inst., Pittsburgh, PA, 1990, pp. 583–589.

[12]Meier, W., Vyrovov, A. O., Bergmann, V., and Stricker, W., "Simultaneous Raman/LIF Measurements of Major Species and NO in Turbulent H_2/Air Diffusion Flames," *Applied Physics B*, Vol. 63, 1996, pp. 79–90.

[13]Antonia, R. A., Prabhu, A., and Stephenson, S. E., "Conditionally Sampled Measurements in a Heated Jet," *Journal of Fluid Mechanics*, Pt. 3, Vol. 72, 1975, pp. 455–480.

[14]Chevray, R., and Tutu, N. K., "Intermittency and Preferential Transport of Heat in a Round Jet," *Journal of Fluid Mechanics*, Pt. 1, Vol. 88, 1978, pp. 138–160.

[15]Lockwood, F. C., and Moneib, H. A., "Fluctuating Temperature Measurements in a Heated Round Free Jet," *Combustion Science and Technology*, Vol. 22, No. 1, 1980, pp. 63–81.

[16]Pitts, W. M., and Kashiwagi, T., "The Application of Laser-Induced Rayleigh Light Scattering to the Study of Turbulent Mixing," *Journal of Fluid Mechanics*, Vol. 141, April 1984, pp. 391–429.

[17]Richards, C. D., and Pitts, W. M., "Global Density Effects on the Self-Preservation Behavior of Turbulent Free Jets," *Journal of Fluid Mechanics*, Vol. 254, Sept. 1993, pp. 417–435.

[18]Birch, A. D., Brown, D. R., Dodson, M. G., and Thomas, J. R., "Turbulent Concentration Field of a Methane Jet," *Journal of Fluid Mechanics*, Vol. 88, Pt. 3, 1978, pp. 431–449.

[19]Dyer, T. M., "Rayleigh Scattering Measurements of Time-Resolved Concentration in a Turbulent Propane Jet," *AIAA Journal*, Vol. 17, 1979, pp. 912–914.

[20]Gouldin, F. C., Schefer, R. W., Johnston, S. C., and Kollmann, W., "Nonreacting Turbulent Mixing Flows," *Progress in Energy and Combustion Science*, Vol. 12, No. 4, 1986, pp. 257–303.

[21]Schefer, R. W., and Dibble, R. W., "Conditional Sampling of Velocity in a Turbulent Nonpremixed Propane Jet," *AIAA Journal*, Vol. 25, No. 10, 1987, pp. 1318–1330.

[22]Dibble, R. W., Hartmann, V., Schefer, R. W., and Kollmann, W., "Conditional Sampling of Velocity and Scalars in Turbulent Flames Using Simultaneous LDV-Raman Scattering," *Experiments in Fluids*, Vol. 5, No. 2, 1987, pp. 103–113.

[23]Barlow, R. S., *Proceedings of the Third International Workshop on Measurements and Computation of Turbulent Nonpremixed Flames*, URL: http://www.ca.sandia.gov/tdf/Workshop [1998].

[24]Johnston, S. C., Dibble, R. W., Schefer, R. W., Ashurst, W. T., and Kollmann, W., "Laser Measurements and Stochastic Simulations of Turbulent Reacting Flows," *AIAA Journal*, Vol. 24, 1986, pp. 918–937.

[25]Biringen, S., "An Experimental Study of a Turbulent Axisymmetric Jet Issuing into a Coflowing Airstream," von Kármán Inst. for Fluid Dynamics, TN 110, 1975.

[26]Dahm, W. J. A., and Dibble, R. W., "Coflowing Turbulent Jet Diffusion Flame Blowout," *Twenty-Second Symposium (International) on Combustion*, Combustion Inst., Pittsburgh, PA, 1988, pp. 801–808.

[27]Pitts, W. M., "Effects of Global Density Ratio on the Centerline Mixing Behavior of Axisymmetric Turbulent Jets," *Experiments in Fluids*, Vol. 11, No. 2/3, 1991, pp. 125–134.

[28]Pitts, W. M., "Reynolds Number Effects on the Mixing Behavior of Axisymmetric Turbulent Jets," *Experiments in Fluids*, Vol. 11, No. 2/3, 1991, pp. 135–141.

[29]Bilger, R. W., Antonia, R. A., and Sreenivasan, K. R., "Determination of Intermittency from the Probability Density Function of a Passive Scalar," *Physics of Fluids*, Vol. 19, No. 10, 1976, pp. 1471–1474.

J. P. Gore
Associate Editor